SPIRALS IN EXCITABLE MEDIA FROM HALF PLANE WAVES : AN ASYMPTOTIC VIEW

Vincent Hakim

Laboratoire de Physique Statistique
24 rue Lhomond, 75231 Paris Cedex 05, France

Abstract

Spiral waves are remarkable structures observed in two-dimensional excitable media. They can be understood as deformations of half plane waves in the regime where the wave tip rotates on a circle which is much larger than the width of the one-dimensional pulse. We describe an asymptotic analysis of spirals and of their counterparts, retracting waves, from this viewpoint, in the free boundary limit where the propagating excited region is bounded by a sharp interface. Spiral drift in an imposed electric field is also described as an example of application of the analysis.

1 Introduction

Excitable media are monostable media in which a small but finite perturbation can generate a large excursion in the medium state before it returns to its stable state. This property allows the propagation of nonlinear solitary waves in the medium with one excursion at a given place acting as a perturbation of the neighboring locations and driving subsequent excursions. The proeminent (quasi) one dimensional example of a neuron axon, as originally described by Hodgkin and Huxley [1] for the squid giant axon, can serve as an illustrative example. In the steady stable state, the axon interior is at a more negative potential than the exterior medium. For a small membrane depolarization (< 6.5 mV for the squid axon), nothing special happens, the membrane potential returns to its stable rest value in a monotonous way. On the contrary, for a depolarization greater than 6.5 mV, the membrane potential first increases dramatically, reaching a positive value of about $+30$ mV before returning to its stable negative value. The electric spread of this large depolarization of one membrane segment is sufficient to trigger large excursions in the membrane potential of neighboring membrane segments and this allows the propagation of the axon potential as a solitary depolarization wave along the axon[1].

Besides the important case of the action potential, other classic one-dimensional (or quasi one-dimensional) examples include the propagation of electrochemical waves along iron wires bathed in acid, [2], and electric activity in a ring of heart tissue [3, 4].

Wave propagation becomes even more interesting in an excitable medium of higher dimension [5, 6]. We will here restrict our attention to a two dimensional situation like the propagation of chemical waves in a shallow chemical medium in a Petri dish [7] [2] or the propagation electrical activity in a thin slice of heart tissue[10]. As expected from the one dimensional case, one can observe the propagation of planar and circular waves. More interestingly, one also observe spiral waves[11]. These beautiful structures have originally mostly been studied using the Belousov-Zhabotinsky chemical reaction (although observations were also made with the Fe/acid system [12]). They have now been analysed in other contexts as different as catalytic oxydation on a metal surface[13] and aggregation of amobae colonies [14]. Much of the interest in these exotic waves also come from their suspected role in different kinds of cardiac arrhythmias and as potential precursor of ventricular fibrillation[15].

Mathematical models of excitable media range from very simplified descriptions, as the original cellular automata of Moe et al. [16], to quite complex ones, like some of the recent refinements of the original Hodgkin and Huxley proposal which includes several types of ions channels and ion pumps to model electrophysiology as accurately as possible [17]. We describe here a two-variable reaction-diffusion model originally proposed [18] as a simplification of the Hodgkin-Huxley four-variable description,

$$
\begin{aligned}
\partial_t u &= \epsilon \nabla^2 u + f(u,v)/\epsilon \\
\partial_t v &= g(u,v)
\end{aligned}
\tag{1}
$$

For definiteness, we choose $f(u,v) = 3u - u^3 - v$, $g(u,v) = u - \delta$, with

[1] Identifying the precise molecular mechanisms underlying the Hodgkin-Huxley description has been one of the main tasks of electrophysiology during the last fifty years. The interested reader can consult B. Hille *Ion channels of excitable membranes* (1992, Sinauer Associates, Inc, Sunderland, Mass) for (much) more information.

[2] In the better controlled modern versions, the reaction takes place in a porous medium (a gel or a thin porous glass disk) fed by one (or two) reactor where the reagent are constantly stirred [8, 9].

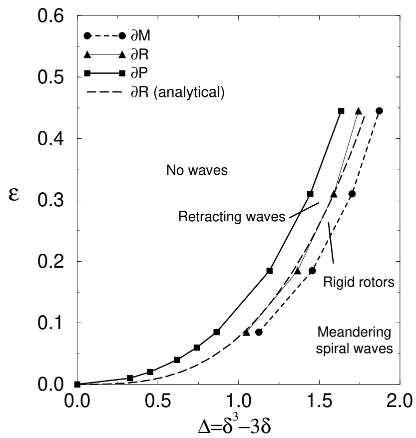

Figure 1: The different modes of wave propagation in the parameter space ϵ (the ratio of the fast u to the slower v time scale) and Δ (defined as $v_s - v_0$). The kinetics of u and v are given by $f(u,v) = 3u - u^3 - v,\ g(u,v) = u - \delta$.

$-\sqrt{3} < \delta < -1$ and the single rest state $u_0 = \delta,\ v_0 = 3\delta - \delta^3$. This model has since often been used and it has been found to give a reliable semi-quantitative description in different contexts with mild variations in the choice of the functions f and g [19]. Numerical surveys of parameter space [20, 21] show that the type of wave which can propagate depends on the choice of the constants ϵ and δ.

In Fig. 1, one dimensional solitary wave propagation is not possible in the whole region marked "no wave", above the line marked ∂P, using the terminology introduced in [21]. Below the line ∂P, a one-dimensional pulse (as well as a 2D planar pulse) can propagate as shown in Fig. 2. However, just below the line ∂P, a *half* plane wave (obtained by cutting in two a plane wave and matching smoothly one of the two halves to the rest state) is found to retract as it propagates, as shown on Fig. 3.

This persists in the whole region between the lines ∂P and ∂R. Exactly on the line ∂R, a half plane wave of well defined shape propagates without retracting or growing. Below the line ∂R, a half plane wave transforms into a

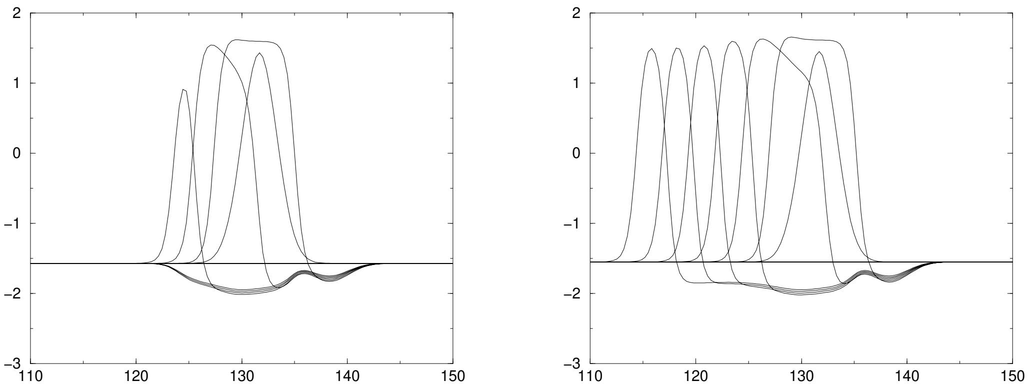

Figure 2: Propagation in one dimension. a) Left: above the line ∂P ($\epsilon = .1$, $\delta = -1.57$ i.e. $\Delta = 0.840$) propagation fails. b) Right: Below the line ∂P ($\epsilon = .1$, $\delta = -1.55$ i.e. $\Delta = 0.926$) a one dimensional pulse (or a two dimensional plane wave) propagates toward the left. In both cases, the u field is represented every $\Delta t = 5$ starting from the initial condition at $t = 0$ (the gaussian waveform centered around $x \simeq 131.5$) up to $t = 30$ (the initial gaussian v field (not represented) is centered around $x \simeq 138$; the shift between the two initial fields induces the leftward propagation).

steadily rotating spiral wave. Farther below ∂R lies the Hopf bifurcation line ∂M on which the steady rotation turns into the two- frequency "meandering" spirals. Still farther below ∂M, the wave motion becomes more complex and possibly chaotic [21] in a still poorly characterized "hypermeander" region (not shown in Fig. 1).

We outline below, some work [22, 23, 24, 25, 26, 27] which aims at providing insights into the phase diagram of Fig. 1 by performing an asymptotic analysis of its lower left hand corner, that is in the limit $\epsilon \to 0$, $\Delta \to 0$. A detailed account can be found in [27].

2 One-dimensional pulses

We start with the well-known case of the one-dimensional pulses. The time scale of the u- equation (1) is of order ϵ and much shorter than the time scale of the the v-equation (1) for small ϵ. It is therefore useful to first consider the dynamics of u, Eq. (1), with v constant and equal to the rest state value

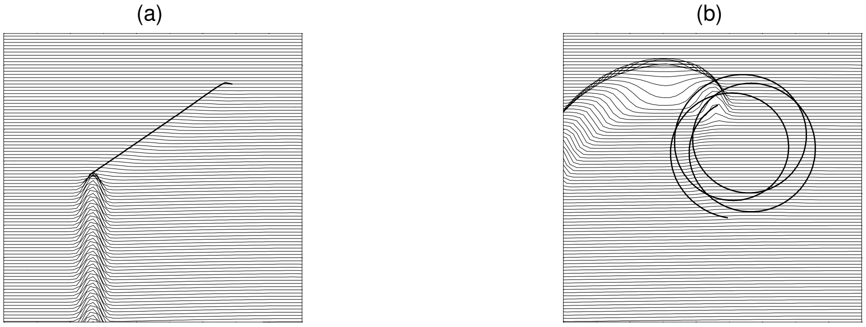

Figure 3: Surface plots of u illustrating (a) a retracting wave for $\delta = -1.4$ and $\epsilon = 0.27$, in between the ∂P and ∂R boundaries. The wave propagates to the left (west) and the wave tip propagates toward the southwest (the thick solid line is the wave tip trajectory) (b) a large core meandering spiral wave for $\delta = -1.4$ and $\epsilon = 0.18$, close to the ∂M boundary. The wave tip trajectory (thick solid line) is not a simple circle.

$v_0 = 3\delta - \delta^3$,

$$\partial_t u = \epsilon \nabla^2 u - \partial_u P/\epsilon \tag{2}$$

with $P(u) = -3u^2/2 + u^4/4 + vu$. This is simply the well-studied bistable Ginzburg-Landau equation. It has two stable equilibrium points, $u_0 = \delta$ and $u_1 = [-\delta + \sqrt{12 - 3\delta^2}]/2$, and front solutions which connect u_0 and u_1. With $-\sqrt{3} < \delta < -1$, a front moves at the velocity $c(v)$ such that the u_1-state invades the u_0-state. The velocity $c(v)$ is a monotoneously decreasing function of v with $c(0) = 0$ (i.e. the Maxwell or "stall" value is $v_s = 0$) and $c(v) = -\alpha v$ with $\alpha = 1/\sqrt{2}$ for $|v| \ll 1$ with our choice of function f. How is the dynamics of such a front modified by taking the evolution of v into account? the front passage at a given point produces a jump in the value of u from u_0 to u_1 in a time of order ϵ/c that is too small to produce a notable change of v (if c is not very small). However, after the front passage, v increases on a time scale of order unity. When v has grown sufficiently, the u_0-state becomes the preferred state and a second front connecting back the u_1-state to the u_0-state follows the first one. The width W of the excited zone between the two fronts is just such that during the time W/c between the passage of the two fronts, v grows from from v_0 to $-v_0$ (this is a stable state since if the width between the two fronts is bigger than W, v grows past $-v_0$ and the second front moves faster than the first one i.e. the width between the two fronts diminishes).

This simple description of the excitable pulse in the small ϵ limit needs to be refined when c is small enough (i.e. W is small enough) for the interaction between the two fronts to become important, a case which we now consider. For $|v_0| \ll 1$ (i.e. $\delta \simeq -\sqrt{3}$), we anticipate (and check at the end) that $|v|$ will remain small in the whole pulse and that u will stay close to $\sqrt{3}$ in the excited zone $\mathcal{D}^+$. So, the dynamics of v in $\mathcal{D}^+$ can be taken simply to be

$$\partial_t v = 1/\tau_e \tag{3}$$

with $\tau_e = 1/(u_1 - \delta) = 1/(2\sqrt{3})$. Two Ginzburg-Landau fronts at the Maxwell point have an attractive interaction which decreases exponentially with distance. With the notation of Eq. (2), it reads [28] for two fronts located at x_1 and $x_2 < x_1$ (with $u(x) \simeq u_1$ for $x_2 < x < x_1$)

$$\frac{dx_2}{dt} = -\frac{dx_1}{dt} = \beta \exp[\sqrt{P''(u_1)}(x_2 - x_1)/\epsilon] \tag{4}$$

and $\beta = 12\sqrt{6}$ with our choice of f [3]. For the leading (x_1) and trailing (x_2) fronts bounding the excited zone of a pulse moving at velocity c, one therefore obtains

$$\frac{dx_1}{dt} = c \;=\; -\alpha\, v_0 - \beta \exp[\sqrt{P''(u_1)}(x_2 - x_1)/\epsilon] \tag{5}$$

$$\frac{dx_2}{dt} = c \;=\; \alpha\,(v_0 + \frac{x_1 - x_2}{\tau_e\, c}) + \beta \exp[\sqrt{P''(u_1)}(x_2 - x_1)/\epsilon] \tag{6}$$

The sum of (5) and (6) relates the pulse width $W = x_1 - x_2$ to its velocity, $W = 2\tau_e c^2/\alpha$. Eq. (5) thus reads

$$-\alpha\, v_0 = c + \beta \exp[-\sqrt{P''(u_1)}\frac{2\tau_e}{\alpha\epsilon}c^2] \equiv S(c) \tag{7}$$

This expression is meaningful only if W, the width of the pulse, is much larger than ϵ, the width of the fronts, that is for $c \gg \epsilon$. For this range of c, the function S(c) on the r.h.s of (7) has a single minimum at $c^* \sim \sqrt{-\alpha\epsilon\log(\epsilon)/(4\tau_e\sqrt{P''(u_1)})} \sim \sqrt{-\epsilon\log(\epsilon)/2}$ and $S(c^*) \sim c^*$. So, for $-\alpha v_0$ larger than $S(c^*)$ there exist two steady pulses, a larger (stable) one which corresponds to the one described above, and a smaller (unstable) one which is due to the attractive interaction between the fronts. These two steady states merge and disappear in a saddle-node bifurcation when $-\alpha v_0$ becomes smaller than $S(c^*)$. This explains the line ∂P for small ϵ and gives its asymptotic behavior $\Delta \sim S(c^*)/\alpha \sim \sqrt{-\epsilon\log(\epsilon)/2}$ (using the notations of Fig.1).

[3] The front location should be defined in a precise and consistent (but arbitrary) way for the exponential prefactor to be meaningful in Eq. 4. We choose here to locate the front at the point where $u = 0$. The constant β is explicitly given by

$$\beta = \frac{2\kappa^2 P''(u_1)}{\epsilon \int_{-\infty}^{+\infty} dx (\partial_x u_f)^2}$$

It is related to the prefactor κ of the exponential approach to u_1 for a front $u_f(x)$ located at $x = 0$ and connecting u_0 at $x = -\infty$ to u_1 at $x = +\infty$,

$$u(x) - u_1 \sim -\kappa \exp[\sqrt{P''(u_1)}x/\epsilon], \text{ for } x \gg 1$$

With our choice of f, the front solution at the Maxwell point is $u_f(x) = \sqrt{3}\tanh(\sqrt{3/2}x/\epsilon)$ and one obtains for the different constants $u_1 = \sqrt{3}$, $P''(u_1) = 6$, $\kappa = 2\sqrt{3}$ $\epsilon \int_{-\infty}^{+\infty} dx(\partial_x u_f)^2 = 2\sqrt{6}$. This gives the value $\beta = 12\sqrt{6}$ quoted above.

3 Two-dimensional waves and the line ∂R

3.1 The sharp boundary limit in two dimensions

As seen in the previous section, in the small-ϵ limit, the one dimensional pulse can be viewed as the propagation of an excited zone bounded by two fronts moving at the velocity $c(v)$ where v is the local value of the field v at the front/back interface. This view can be simply extended to a propagating two-dimensional wave with the difference that the local velocity of the bounding interface now depends on its curvature. When the bounding interface is curved on a length scale long compared to its width, one has

$$c_n = c(v) - \epsilon\,\kappa \tag{8}$$

which is simply (biased) motion by curvature. The field v evolves as in the one dimensional case. We assume that only values close to the Maxwell point will matter in the small-ϵ limit, so the dynamics of v is simply,

$$\begin{aligned} \partial_t v &= 1/\tau_e \quad \text{ in } \mathcal{D}^+ \qquad (9) \\ \partial_t v &= -(v - v_0)/\tau_R \quad \text{ in } \mathcal{D}^- \qquad (10) \end{aligned}$$

where $\mathcal{D}^+$ denotes the excited zone and $\mathcal{D}^-$ the recovery region. As first shown in [22], different kind of steady waves can be easily determined in the small-ϵ limit using Eq. (8) and (9,10).

3.2 The line ∂R

The line ∂R of existence of steady half plane wave can be first determined. Using rotational invariance, one searches, without loss of generality, for a steady shape which propagates along the y-direction at the same velocity as a plane wave, with the medium in the rest state (u_0, v_0) for $x \to \infty$. In the small-ϵ limit, this reduces to finding the front and back interfaces of the propagating excited zone. The front interface propagates in the undisturbed medium and therefore, it obeys Eq. 8 with $c(v_0) = c_0$,

$$\frac{d^2Y_f}{dx^2} = \left[1 + (\frac{dY_f}{dx})^2\right] - \left[1 + (\frac{dY_f}{dx})^2\right]^{3/2} \tag{11}$$

where ϵ/c_0 has been used as length unit and the front interface shape as been parametrized (and adimensionned) as $Y_f(x)$. In the excited zone, the field v

increases from $v = v_0$ on the front interface to $v_0 + \epsilon(Y_f(x) - Y_b(x))/c_0^2\tau_e$ on the back interface using Eq. (9). Therefore, Eq. 8 gives for the shape $Y_b(x)$ of the back interface

$$\frac{d^2Y_b}{dx^2} = \left[1 + (\frac{dY_b}{dx})^2\right] + [1 - B\,[Y_f(x) - Y_b(x)]]\left[1 + (\frac{dY_b}{dx})^2\right]^{3/2} \tag{12}$$

where $B = \epsilon/(\alpha^2\tau_e\Delta^3)$. The boundary conditions at infinity are simply

$$\frac{dY_f}{dx}|_{x=+\infty} = \frac{dY_b}{dx}|_{x=+\infty} = 0 \tag{13}$$

Translation invariance allows us to fix the wave tip[4] at $x = y = 0$ and we require as other boundary conditions

$$Y_f(0) = Y_b(0) = 0, \quad dY_f/dx(0) = -dY_b/dx(0) = +\infty \tag{14}$$

.

Eq. (12) can be integrated without any supplementary condition (analytically, in fact). On the contrary, a simple shooting argument shows that the boundary conditions on Eq. (12) can only be satisfied for a special value B_c of B. Numerically, one finds $B_c = 0.5353\cdots$ [23]. Recalling the definition of the parameter B, this determines the asymptotic equation of the line ∂R as $\Delta \sim (\epsilon/\alpha^2\tau_e B_c)^{1/3}$. This justifies a posteriori the approximation of the v-dynamics by its limiting form (9, 10) in the vicinity of the Maxwell point.

4 Away from ∂R

Away from the line ∂R, the simple half plane waves propagating at the plane wave velocity c_0 of the previous section do not exist anymore. However in the vicinity of ∂R, the shapes of the propagating waves remain close in their tip region to a half plane wave of a neighboring point on the line ∂R. Far from the tip region, they can on the contrary be approximated by the one-dimensional pulse with a weak and slowly varying transverse curvature. This motivates a perturbative approach in which a tip region is matched on an intermediate scale to a far tip region.

[4]For the PDE model (1,1), the wave tip can be arbitrarily defined as a point of zero normal velocity on an iso-u line corresponding to a u-value intermediate between the rest and excited state (say $u = 0$, for our choice of functions). In the sharp interface limit, it is simply the point of zero normal velocity on the interface.

4.1 The tip region

For a medium with kinetic parameters close but away from ∂R, the velocity c_t of motion of the tip region can be determined as follows [24, 25]. In a reference frame with its y-axis aligned with the tip tangential velocity c_t, the wave steady front and back interfaces, $y_f(x)$ and $y_b(x)$, obey

$$\frac{d^2y_f}{dx^2} = \frac{c_t}{c_0}\left[1+(\frac{dy_f}{dx})^2\right] - \left[1+(\frac{dy_f}{dx})^2\right]^{3/2} \tag{15}$$

$$\frac{d^2y_b}{dx^2} = \frac{c_t}{c_0}\left[1+(\frac{dy_b}{dx})^2\right] + \left[1-B\frac{c_0}{c_t}\left[y_f(x)-y_b(x)\right]\right]\left[1+(\frac{dy_b}{dx})^2\right]^{3/2} \tag{16}$$

As before, ϵ/c_0 has been used as length unit. For $|B-B_c| \ll 1$ and anticipating that $|c_t/c_0 - 1| \ll 1$, Eq.(15, 16) can be linearized around the half plane wave shape as $y_f = Y_f + \delta y_f, y_b = Y_b + \delta y_b$ with $\delta B = B - B_c$ and $\delta c = c_t - c_0$. This gives linear equations in the form

$$\mathcal{L}_f(\delta y_f) = \mathcal{I}_f[\delta c_t/c_0; Y_f(x)] \tag{17}$$

$$\mathcal{L}_b(\delta y_b) = \mathcal{I}_b[\delta c_t/c_0, \delta B, \delta y_f; Y_f(x), Y_b(x)] \tag{18}$$

where the linear operators $\mathcal{L}_f$ and $\mathcal{L}_b$ are second order differential operators with coefficients which depend on Y_f and Y_b. The right hand inhomogeneous members I_f and I_b also depend linearly on $\delta c_t/c_0$ and, for I_b, on $\delta B, \delta y_f$. Imposing the wave tip position ($y_f = y_b = 0$) fixes the boundary conditions at $x = 0$ and uniquely determines δy_f and δy_b. Integration of Eq.(17) provides a δy_f polynomially growing with x (i.e. $y_f(x) \sim x^2/6\ \delta c_t/c_0$ as $x \to +\infty$) which can be matched to the far tip intermediate region, as shown below. On the contrary, $\mathcal{L}_b$ reduces to $d^2/dx^2 - B_c$ for large x and in general δy_b grows exponentially like $\exp(\sqrt{B_c}\,x)$ on distances of order one from the tip. It is only when $\delta c_t/c_0$ is precisely related to δB that the exponential growth is absent and that δy_b can grow algebraically like δy_f. After noting that the adjoint $\mathcal{L}_b^\dagger$ possesses a zero mode $\xi(x)$ which vanishes exponentially as $x \to +\infty$, the relation between $\delta c_t/c_0$ and δB is conveniently obtained as a solvability condition

$$\int_0^{+\infty} dx\, \xi\, \mathcal{I}_b = 0 \tag{19}$$

The linear dependence of $\mathcal{I}_b$ on δB and $\delta c_t/c_0$ gives after explicit evaluation of (19)

$$\frac{c_t}{c_0} = 1 + \frac{B-B_c}{K} \text{ with } K \simeq .63 \tag{20}$$

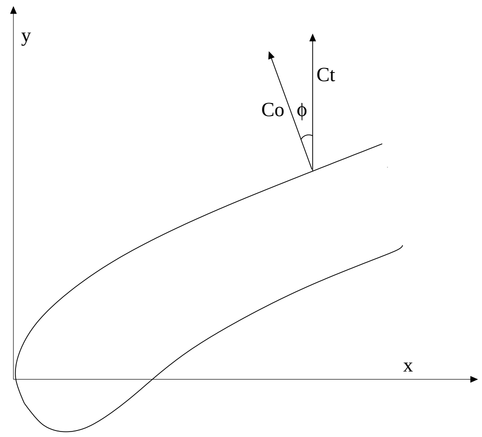

Figure 4: Sketch of a retracting wave seen as a steady wave in a referential moving at the tip velocity.

Therefore, one obtains that the tip velocity c_t is larger than the plane wave velocity c_0 for $B > B_c$ whereas it is smaller for $B < B_c$. This gives rise to two different wave types on each side of ∂R.

4.2 Above the line ∂R ($B > B_c$): the retracting waves

When $B > B_c$, the tangential tip velocity c_t is larger than the velocity of plane waves. This can be achieved by an asymptotically straight steady half plane wave when the asymptotic straight part is not orthogonal to the tangential tip velocity but inclined at an angle ϕ such that $c_0 = c_t \cos(\phi)$ (see Fig.4.1). Indeed, explicit integration shows that, for $c_t/c_0 > 1$, Eq.(15) possess just such a solution which asymptotically obey $dy_f/dx(+\infty) = \sqrt{(c_t/c_0)^2 - 1}$. This steady half plane wave is nothing else than a retracting wave viewed in a reference frame which moves at the tip tangential velocity.

4.3 Below the line ∂R ($B > B_c$): the spiral waves

For $B < B_c$, the tangential tip velocity c_t is smaller than the plane wave velocity c_0. This cannot be achieved by a steadily translating asymptotically straight wave. The velocity difference induces a rotation (see Fig.4.3) of the wave tip region which is almost rigid on a length $\ell \sim \epsilon/(c_0\sqrt{1 - c_t/c_0})$ where the curvature dependance of the normal velocity (8) is the dominant effect.

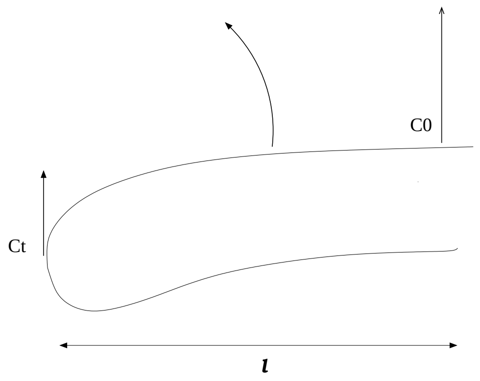

Figure 5: Sketch of the rotation of the spiral tip region induced by the velocity difference between the near and far tip region

The subsequent outward propagation of the wave produces the characteristic spiral shape. This can be simply analyzed by assuming that the wave is steady in a referential rotating at the frequency ω_1. For the front spiral interface, Eq.(8) reads in polar coordinates (assuming a counterclockwise rotation for definiteness),

$$\frac{d\psi}{d\rho} = \rho\Omega[1+\psi^2] - [1+\psi^2]^{3/2} - \frac{\psi(1+\psi^2)}{\rho} \tag{21}$$

where we have defined $\psi = r\, d\theta_f/dr$ and rescaled r as $r = \rho\epsilon/c_0$ to make it clear that Eq. (21) depends on the single dimensionless parameter $\Omega = \omega_1\epsilon/c_0^2$. The boundary condition at infinity is $\psi \sim -r\omega_1/c_0$. It has been assumed in Eq. (15) that the spiral propagates in the medium rest state i.e. that v has returned to the rest value v_0 after the previous wave passage. It can be checked afterwards that the spiral period diverges near ∂R so that the assumption is self-consistent. One can note that Eq. (21) is identical to a classic equation for the growth of screw dislocations on crystal surfaces [29]. Eq. (21) with the chosen boundary condition at infinity uniquely determines ψ_f. For $0 < \Omega < .331$, ones finds that ψ is well defined for ρ in $]\rho_0, +\infty[$ with $\psi \to +\infty$ at $\rho = \rho_0$. ρ_0 is the location of the spiral tip and is found to increase from 0 to $+\infty$ when Ω decreases from .331 to 0. The limit $\Omega \to 0$ is the limit of interest here and it can be analyzed by matching three regions:
- Far from the spiral tip, the curvature correction to the normal velocity in

Eq.(8) becomes negligible and Eq. (21) reduces to

$$z\frac{d\theta_{out}}{dz} = -\sqrt{z^2-1} \tag{22}$$

with $r = zc_0/\omega_1$, which can be simply integrated.
-On distance of order ϵ/c_0 from the spiral tip, Eq. (21) reduces to the previous Eq. (15) by introducing $\rho = \rho_0 + x$ and $y\epsilon/c_0 = r_0\theta_f$ and identifying $\omega_1 r_0$ as the tangential tip velocity.
-These two regions join in an intermediate region where the interface curvature is small and the interface tangent almost radial (i.e $\psi \ll 1$).

As shown in detail in Appendix A, matching these regions gives the first terms of the asymptotic expansion of the spiral tip position ρ_0 in the limit $\Omega \to 0$

$$\rho_0 = \frac{1}{\Omega} - b\frac{1}{\Omega^{1/3}} + b_2 - b_3\Omega^{1/3} + \cdots \tag{23}$$

with $b = -2^{1/3}a_1 \simeq 2.9458\cdots$ (a_1 being the first zero of Airy function Ai), $b_2 = 1 + \pi/2 \simeq 2.507\cdots$ and $b_3 \simeq 4.339$ is given by a definite integral of Airy function (Eq. (40,45)). The first two terms of (23) are sufficient to obtain the leading divergent behavior of the spiral core radius R_0 as $c_t/c_0 \to 1$. Returning to the original units, one obtains

$$R_0 = \frac{\epsilon}{c_0}\left(\frac{bc_0}{c_0 - c_t}\right)^{3/2} \tag{24}$$

Comparing with the previous relation (20) determines the spiral radius and frequency close to the line ∂R,

$$R_0 = \frac{\epsilon}{c_0}\left(\frac{bK}{B_c - B}\right)^{3/2}, \quad \omega_1 = \frac{c_0^2}{\epsilon}\left(\frac{B_c - B}{bK}\right)^{3/2} \tag{25}$$

5 Dynamics: drift in an external field

In the previous section, the steady spiral solutions of Eq. (1) have been obtained in the vicinity of the line ∂R. It was realized in [26] and [27] that the analysis could be generalized without too much difficulty to capture dynamic phenomena such as meander and spiral drift in a field [5]. The underlying idea

[5] The instability of multi-armed spirals is also considered in [27].

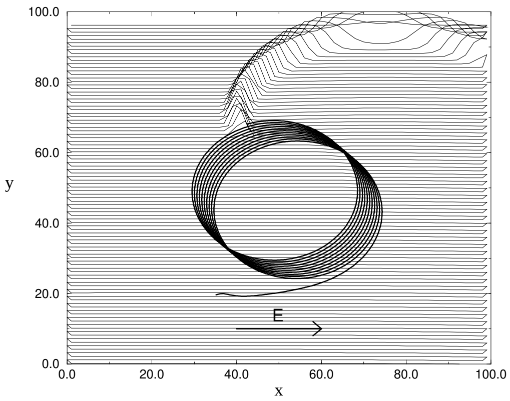

Figure 6: Simulation of the FN model of Fig. 1 ($\epsilon = 0.185, \delta = -1.41$) with an external field added as in Eq. (26) with $E = 1.0\ 10^{-3}$. The wave tip trajectory is shown (bold line) as well as surface plots of u showing the spiral position at the end of the simulation.In this large core regime, the spiral is found to drift at about 135° with the field in good agreement with the asymptotic prediction of $132, 5°$.

is quite simple: when the time dependent phenomenon varies on a sufficiently long time scale then the tip motion can be analyzed in an "adiabatic" way. Namely, the tip motion is characterized by its tangential velocity and its instantaneous rate of rotation which are themselves obtained as functions of the *instantaneous* state of the medium in the tip region exactly as for for steady states. In other words, the tip moves at each instant as the tip of a steady spiral.

We illustrate, here, the idea by describing the analysis of spiral drift in the presence of an external field $\mathbf{E}$ which couples to u. Eq.(1) then becomes

$$\partial_t u = \epsilon\, \nabla^2 u + f(u,v)/\epsilon - \epsilon \mathbf{E}.\nabla u \tag{26}$$

As shown in Fig. 6, the field $\mathbf{E}$ induces a drift of spiral waves at a well defined and non-trivial angle with the field. In order to explain this using the previous analysis of spiral waves, we first note that the eikonal equation (8) is modified to

$$c_n = c(v) - \epsilon\, \kappa + \epsilon \mathbf{n} \cdot \mathbf{E} \tag{27}$$

For a weak field, the supplementary term in (27) as compared to (8) can be treated in perturbation. Linearizing around the half plane wave shape $Y_f(x), Y_b(x)$ and proceeding as in section 4.1 one obtains the generalization of Eq. 20 which includes the field $\mathbf{E}$,

$$c_t = c_0 + c_0\frac{B-B_c}{K} + (1+\gamma_{||})\,\epsilon E_{||} + \gamma_{\perp}\,\epsilon E_{\perp} = c_t^0 + (1+\gamma_{||})\,\epsilon E_{||} + \gamma_{\perp}\,\epsilon E_{\perp} \quad (28)$$

The constants $\gamma_{||}$ and $\gamma_{\perp}$ have definite expressions coming from the evaluation of the solvability condition which give $\gamma_{||} = -B_c/K \simeq -0.850$ and $\gamma_{\perp} \simeq 0.929$. Most importantly, the field components which appear in (28) are the instantaneous projections of the field on the axes of a frame linked to the spiral tip, namely $E_{||}$ is the projection of E on the tangential tip velocity (the y axis) and $E_{\perp}$ the orthogonal component (the projection on the x axis). So, they oscillate at the spiral rotation frequency ω_1, $E_{||} = -E\sin(\omega_1 t)$ and $E_{\perp} = E\cos(\omega_1 t)$.

Eq. (28) gives the instantaneous velocity of the spiral tip along its trajectory. The tip motion is determined in addition by the instantaneous curvature R_i of the trajectory (the instantaneous spiral core radius) which depends on the difference between the tangential tip velocity and the actual velocity of the far tip part in the presence of the field $\mathbf{E}$ i.e. $c_0 + \epsilon E_{||}$. Similarly to Eq.(24), one obtains to linear order

$$\delta R_i \equiv R_i - R_0 = \frac{3}{2}\frac{\gamma_{||}\epsilon E_{||} + \gamma_{\perp}\,\epsilon E_{\perp}}{c_t^0 - c_0}\, R_0 \quad (29)$$

Determining the motion of the spiral tip thus reduces to the kinematic problem of finding the motion of a point, being given its instantaneous velocity and the instantaneous curvature of its trajectory. Simply considering here linear displacements from the unperturbed circular trajectory $x = (R_0 + \delta r(t))\cos(\omega_1 t + \psi(t)), y = (R_0 + \delta r(t))\sin(\omega_1 t + \psi(t))$, one obtains

$$\frac{d^2 r}{dt^2} + \omega_1^2 r = \omega_1^2 \delta R_i \quad (30)$$

Without a field, $\delta R_i = 0$ and (30) simply reflects the harmonic behavior of the tip displacement of a steady spiral slightly translated with respect to the reference unperturbed spiral. The field perturbation acts *via* δR_i (Eq. 29) as a forcing of the translation modes. Since here the forcing is resonant with the frequency of the l.h.s harmonic equation, it induces a linear growth of the displacement r that is a linear spiral drift. The spiral drift angle θ_D with the external field is simply obtained as

$$\tan(\theta_D) = \gamma_\perp / \gamma_\parallel \tag{31}$$

The idea can be applied to treat other dynamical effects. One obtains the same harmonic oscillator equation (30) but the forcing term depends on the particular effect under consideration. For example, it is shown in [27] that the meander instability arises from the spiral tip interaction with itself induced by the incomplete relaxation of the v field to the rest value v_0 during one spiral rotation. This gives rise to a r.h.s forcing in Eq. (30) of the form $F(r(t) - r(t-T))$ that transforms (30) into a delayed differential equation (T being the spiral period).

The relaxation time of the slowest modes of the unperturbed spiral other than the translation and rotation modes is estimated in [27] to be $T(\epsilon/(c_0 R_0))^{1/3}$ which is short compared to the spiral period T for large core spirals. This justifies the basic simplifying idea of using an "adiabatic" approximation for dynamical phenomena which vary on the time scale of the spiral period.

6 Conclusion

The asymptotic analysis summarized above provides a simple picture of spiral wave near the line ∂R and offers a way to deal with different dynamic phenomena. Several remaining questions appear worth of further investigations.

The main element of our analysis is the proximity of the line ∂R where the spiral core diverges. We have in addition focused on the limit $\epsilon \to 0$ because the reduction to a free boundary problem simplifies explicit computations (and also because it is only for small ϵ that the meander instability occurs for large core spirals). However, generalization to the whole line ∂R seems possible if one is willing to deal with the full 2d nature of the near spiral tip region away from $\epsilon = 0$ (the eikonal equation and allied BCF equation will still describe the spiral in the far tip region).

Characterizing and understanding better the region below ∂M seems also worth of some interest. What is the small-ϵ asymptotics of the line where the character of meander changes from inward (as in Fig. 3b) to outward petals? Where is the hypermeander line?

Going from two to three dimensions, the spirals are replaced by scroll waves and new instabilities appear [30]. How far can one extend the present analysis to deal with scroll waves?

Finally, all the results presented here come from formal asymptotics or numerical calculations and all remain to be rigourously proven. We hope that this will serve as an encouragement to some mathematically-minded readers.

Acknowledgments I am grateful to Alain Karma for teaching me most of what I know about excitable media and for a very enjoyable collaboration. I am also grateful to Benoît Pier who took part in this project at an early stage and to Hervé Henry with whom it is now continued. I wish to thank Henri Berestycki and Yves Pomeau for inviting me to participate in this interesting and pleasant Cargese Summer School and for their kind insistence on the writing of these notes.

A Asymptotics of the BCF equation

We consider the BCF equation (21) for a spiral front interface moving in a medium in its rest state

$$\frac{d\psi}{d\rho} = \rho\Omega[1+\psi^2] - [1+\psi^2]^{3/2} - \frac{\psi(1+\psi^2)}{\rho} \tag{32}$$

The imposed boundary condition at infinity is $\psi \sim -\rho\Omega$. As stated in the main text, for $0 < \Omega < .331\cdots$, ψ is well-defined on $]\rho_0(\Omega), +\infty[$ and diverges toward $+\infty$ when $\rho \to \rho_0^+$ (i.e. at the spiral tip). We provide here a derivation of the asymptotic expansion (23) of $\rho_0(\Omega)$ for $\Omega \to 0$ since only the first two terms of (23) were given in previous publications [26, 27].

As explained in [26, 27] and in section 4.3, the spiral interface can be separated into three regions when $\Omega \ll 1$.

Far from the spiral tip, ρ varies on length scales of order $1/\Omega$. Using the rescaled variable z with $\rho = z/\Omega$, one can expand ψ in powers of $1/\Omega$. The first term of the expansion is given by Eq. (22) of the main text. This expansion breaks down near $z = 1$ (i.e. in the spiral tip region) where higher order terms in the expansion involve higher derivatives and are more divergent that low order terms, a typical boundary-layer phenomenon.

Near the spiral tip $\rho_0(\Omega)$, on length scales of order one (the wave tip curvature with our notations), Eq. (32) can be expanded in a different way by using the variable x such that $\rho = \rho_0(\Omega) + x$. Eq. (32) becomes

$$\frac{d\psi}{dx} = [1+\psi^2] - [1+\psi^2]^{3/2} + O(\Omega^{2/3}) \tag{33}$$

where we have anticipated that $\rho_0(\Omega)\Omega - 1 = O(\Omega^{2/3})$. Eq. (33) is identical to (11) (with $\psi = dY/dx$). This shows that on length scales of order one, the spiral wave tip is identical to the tip of a half plane wave (up to small corrections). Eq. (33) can be integrated analytically and the solution large x behavior is

$$\psi = \frac{2}{x} - \frac{2+\pi}{x^2} + \frac{6+(2+\pi)^2/2}{x^3} + O(x^{-4}, \Omega^{2/3}) \tag{34}$$

The spiral tip region where the spiral shape is close to a half plane wave and the far zone where the curvature correction to velocity is negligible do not directly match. Matching occurs in an intermediate region where curvature effects on velocity [$d\psi/d\rho$ in Eq. (32)] are comparable to inclination effects on velocity [ψ^2] and to the kinematic increase of velocity with distance due to rotation [$\Omega(\rho - 1/\Omega)$]. This gives $\rho - 1/\Omega \sim \Omega^{-1/3}$ and $\psi \sim \Omega^{1/3}$. We thus define a rescaled variable ξ and a rescaled function ϕ with $\rho = 1/\Omega + \xi(2/\Omega)^{1/3}$ and $\psi = \phi\,(4\Omega)^{1/3}$. After substituting these expressions in Eq. (32) and expanding ϕ in powers of $\Omega^{2/3}$ as $\phi = \phi_0 + (2\Omega^2)^{1/3}\phi_1 + \cdots$, one obtains,

$$\frac{d\phi_0}{d\xi} = \xi - \phi_0^2 \tag{35}$$

$$\frac{d\phi_1}{d\xi} + 2\phi_0\,\phi_1 = 2\xi\,\phi_0^2 - \phi_0 - \frac{3}{2}\phi_0^4 \tag{36}$$

Eq. (35) is a Riccati equation which can be transformed into the linear Airy equation [$f'' = \xi f$]. Matching with Eq. (22) requires $\phi_0 < 0$ for $\xi \to +\infty$. This imposes that the Airy function vanishes at infinity and is proportional to Ai [31],

$$\phi_0(\xi) = \frac{Ai'(\xi)}{Ai(\xi)} \tag{37}$$

A straightforward integration of Eq. (36) then gives

$$\phi_1(\xi) = -\frac{1}{2} - \frac{1}{Ai(\xi)^2}\int_\xi^{+\infty} dw \left[2wAi'(w)^2 - \frac{3}{2}\frac{Ai'(w)^4}{Ai(w)^2}\right] \tag{38}$$

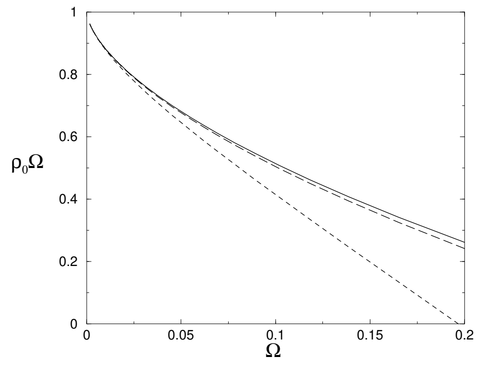

Figure 7: Plot of i) the spiral core radius $\rho_0(\Omega)$ obtained by numerical integration of the BCF equation (32) (bold line) ii) the asymptotic expansion (23) (dashed line) iii) a Pade resummation of this expansion (long-dashed line) $\rho_{0;Pa} = 1 + \Omega^{2/3}\ [-b + (b_2 - bb_3/b_2)\Omega^{1/3}]/[1 + \Omega^{1/3}b_3/b_2] = 1 + \Omega^{2/3}(-2.946 - 2.591\,\Omega^{1/3})/(1 + 1.731\,\Omega^{1/3})$.

Both $\phi_0(\xi)$ and $\phi_1(\xi)$ diverge when ξ tends toward the first zero of Ai, $a_1 = -2.3381\cdots$ [31]. Setting $\xi = a_1 + \eta$, one obtains for the diverging behaviors (note that Airy equation implies $A''(a_1) = 0$),

$$\phi_0(a_1 + \eta) = \frac{1}{\eta} + O(\eta),\ \ \phi_1(a_1 + \eta) = \frac{3}{2\eta^3} + \frac{\gamma_1}{\eta^2} + O(1/\eta) \tag{39}$$

where the constant γ_1 is equal to

$$\gamma_1 = \frac{5}{2A'(a_1)^2}\int_{a_1}^{+\infty} dw\ wAi'(w)^2 \simeq -2.733 \tag{40}$$

In order to obtain the spiral core radius $\rho_0(\Omega)$, it remains to match Eq. (39) and (34). This is done in a usual way by first expressing the outer variable η in terms of the inner variable x and then by requiring that the small η asymptotics of the outer development (39) be identical to the large x asymptotics of the inner developement. Recalling the definition of η and x in terms of the original variable ρ, the first step gives

$$\eta = \left(\frac{\Omega}{2}\right)^{1/3}(\rho_0(\Omega) - \frac{1}{\Omega} - x) - a_1 \tag{41}$$

The expansion of $\rho(\Omega)$ is seeked under the form,

$$\rho_0(\omega) = \frac{1}{\Omega} - b\frac{1}{\Omega^{1/3}} + b_2 - b_3\Omega^{1/3} + \cdots \tag{42}$$

Inserting (42) in (41) gives $b = -2^{1/3} a_1$. Eq. (41) becomes $\eta = (\Omega/2)^{1/3}(x + b_2 - b_3\Omega^{1/3} + \cdots)$. Replacing η by this last expression in (39), expanding for large x and recalling that $\psi = (4\Omega)^{1/3}\phi$, gives the asymptotic expansion

$$\psi = \frac{2}{x} - \frac{2b_2}{x^2} + \frac{6 + 2b_2^2}{x^3} + \Omega^{1/3}\,(2b_3 + 2^{5/3}\gamma_1)(\frac{1}{x^2} - \frac{2b_2}{x^3}) + O(x^{-4}, \Omega^{2/3}) \quad (43)$$

Comparing with the previously obtained large x asymtotics (Eq. (34)) readily gives

$$b_2 = 1 + \pi/2,\ \ b_3 = -2^{2/3}\gamma_1 \simeq 4.339 \quad (44)$$

as announced in the main text. The asymptotic development (23) is compared to $\rho_0(\Omega)$ in Fig. 7.

$$(45)$$

References

[1] A.L. Hodgkin and A. F. Huxley, Nature **144**, 710 (1939); J. Physiol. **117** 500-544 (1952)

[2] W. Ostwald, Zeit. Phys. Chem. **35** 33 (1900); *ibid.***35** 204 (1900).

[3] G. R. Mines, Trans. Roy. Soc. Can. **4**, 43 (1914)

[4] W. E. Garrey, Am. J. Physiol **33** 397 (1914); Physiol. Rev. **4**, 215-250 (1924).

[5] A.T. Winfree, *When Time Breaks Down* (Princeton U. Press, N. J. 1987).

[6] V. S. Zykov, *Modelling of wave processes in excitable media* (Manchester U. Press, Manchester, 1988).

[7] A. N. Zaikin and A. M. Zhabotinsky, Nature **225**, 535 (1970).

[8] Q.Ouyang and H. Swinney, Chaos **1**, 411 (1991); G.S. Skinner and H.L. Swinney, Physica D **48**, 1 (1991).

[9] A. L. Belmonte, Q. Ouyang and J. M. Flesselles, J. Phys. II *France* **7**, 1425 (1997).

[10] J. Davidenko et al., Nature **335**, 349 (1992).

[11] A.T. Winfree, Science **181**, 937 (1973); W. Jahnke, W. E. Skaggs and A. T. Winfree, J. Phys. Chem **93**, 740 (1989).

[12] see R. Suzuki, Adv. Biophys. **9**,115 (1976).

[13] S. Jakubith, H.H. Rotermund, W. Engel, A. von Oertzen and G.Ertl, Phys. Rev. Lett **65**, 3013 (1990).

[14] J. T. Bonner, *The Cellular Slime Molds* (Princeton U. Press, Princeton, 1967); G. Gerisch, Annu. Rev. Biochem. **56**, 853 (1987).

[15] See e.g. the recent focus issue Chaos **8**, vol. 1 (1998)

[16] G. K. Moe, W. C. Rheinboldt and J. A. Abildskov Am. Heart J. **67**, 200 (1964).

[17] D. DiFrancesco and D. Noble, Phil. Trans. R. Soc. Lond. B **307**, 353 (1985); C. Luo and Y. Rudy, Circ. Res. **74**, 1071 (1994).

[18] R. Fitzhugh, Biophys. J. **1**, 445 (1961); J. Nagumo, S. Arimoto and S. Yoshizawa, Proc. I. R. E. **50**, 2061 (1962).

[19] see e.g. R. J. Field and R. M. Noyes, J. Chem. Phys.**60**, 1877 (1974) [Belousov-Zhabotinsky reaction]; [13] [surface catalysis]; L. F. Abbott and E. Marder in *Methods in Neuronal Modeling*, C. Koch and I. Segev, editors (MIT press, Cambridge, Mass, 1998).

[20] V. S. Zykov, Biofizika **31**, 862 (1986).

[21] A.T. Winfree, Chaos **1**, 303 (1991).

[22] P. Pelce and J. Sun, Physica D **48**, 353 (1991).

[23] A. Karma, Phys. Rev. Lett. **66**, 2274 (1991).

[24] A. Karma, in *Nonlinear Phenomena Related to Growth and Form*, M. Ben Amar et al eds, (Plenum Press, N. Y., 1991).

[25] B. Pier DEA report (ENS Lyon, 1995).

[26] V. Hakim and A. Karma, Phys. Rev. Lett. **79**, 665 (1997).

[27] V. Hakim and A. Karma, Phys. Rev. E **60**, 5073 (1999).

[28] A rigorous discussion can be found in J. Carr and R. L. Pego, Comm. Pure Appl. Math. **42**, 523 (1989) who attributes the formula to J. Neu; A simple (but formal) derivation can be found in V. Hakim in *Hydrodynamics and Nonlinear Instabilities*, C. Godrèche and P. Manneville ed. (Cambridge U. Press, Cambridge, 1998) p.328

[29] W.K. Burton, N. Cabrera and F. C. Franck, Phil. Trans. Roy. Soc. (London) **A 243**, 299 (1951).

[30] H. Henry and V. Hakim, Phys. Rev. Lett. **85**, 5328 (2000) and references therein.

[31] *Handbook of Mathematical Functions*, edited by M. Abramowitz and I. A. Stegun (Dover, New York, 1972).